2054 *Macromolecules* **2010**, *43*, 2054–2068
DOI: 10.1021/ma902338m

Macromolecules
ARTICLE

Polymer Adsorption from Bulk Solution onto Planar Surfaces: Effect of Polymer Flexibility and Surface Attraction in Good Solvent

Per Linse* and Niklas Källrot

Physical Chemistry, Center for Chemistry and Chemical Engineering, Lund University, P.O. Box 124, S-221 00 Lund, Sweden

Received October 21, 2009; Revised Manuscript Received December 27, 2009

ABSTRACT: Adsorption of uncharged homopolymers of various flexibilities in good solvent onto planar surfaces at various polymer−surface interaction strengths have been investigated by employing a coarse-grained bead−spring polymer model using simulation techniques. The polymer flexibility ranged from fully flexible to rod-like polymers, and the adsorption strength varied from weak to strong adsorption. Equilibrium adsorption properties were determined by Monte Carlo simulations, and adsorption processes were investigated by Brownian dynamic simulations. In the latter case, the initial systems were composed of a polymer solution and a surface separated by a slab of polymer-free solution. The equilibrium properties of the interfacial systems have been analyzed by monitoring bead and polymer density profiles, number of adsorbed beads and polymers, the components of the radius of gyration perpendicular and parallel to the surface as well as tail, loop, and train statistics. Flexible polymers adsorbed in two layers, and at an increasing surface attraction the number of adsorbed beads and polymers increased and the adsorbed polymers become flatter, whereas rod-like polymers adsorbed in a single and thin layer with a nematic-like order. At increasing polymer stiffness at fixed surface attraction strength, the number of adsorbed beads increased, whereas the number of adsorbed polymers, the polymer extension perpendicular to the surface, and the fraction of beads in tails all displayed nontrivial maxima at similar persistence length. The dynamic analysis showed that the initial adsorption was diffusion controlled, but soon became governed by the probability of a polymer to be captured by the surface attraction. Flexible polymers became flattened after attaching, but their final relaxation mechanism involved an increased perpendicular extension with fewer adsorbed beads and longer tails driven by the surface pressure originating from the surrounding adsorbed polymers. The stiff polymers displayed a much slower final relaxation to their equilibrium state; this relaxation predominately constituting a packing of the rod-like polymers in a 2-dimensional nematic order. Furthermore, we have defined an integration time denoting the adsorption time for adsorbed polymers to become fully integrated into the adsorbed layer. Integration times and residence times of integrated polymers became longer with increasing polymer stiffness and increasing bead−surface attraction.

1. Introduction

Polymers in solution may readily adsorb onto various surfaces where there is an attractive interaction between segments of the polymer and the surface which overcompensates for the conformational entropy loss of the polymer upon adsorption.[1] The adsorption of polymers onto surfaces, weather desired or not, has huge implications in many areas of research. Moreover, understanding and controlling such processes is of great importance and is essential in many different technological aspects ranging from paper industry and paint formulation to pharmaceutical applications,[2] biophysics,[3−5] and nanocomposite materials.[6]

The adsorption process of polymers onto a surfaces is largely governed by the prevailing conditions under which polymer, solvent, and surface interact. The equilibrium adsorbed layer in terms of surface coverage and layer thickness is often of interest from a technical point of view, where a surface is physically or mechanically modified to meet specific requirements. Because of the large number of applications for polymer adsorption, there has historically been a large interest in characterizing layers of adsorbed polymers.[7−11] However, often kinetics is so slow that true equilibrium of the adsorbed polymers may never be achieved on realistic time scales. Resolving the different time scales involved during the entire adsorption process, from diffusional transport to a surface followed by subsequent attachment and spreading on it, thus remains a significant task and a large challenge within the field.

A number of different approaches have been employed to theoretically study the nature of polymer adsorption onto surfaces from bulk solution. Adsorption profiles near adsorbing surfaces have been characterized using mean-field approaches[12,13] as well as using various simulation techniques.[14−17] The dynamics of polymer adsorption has also been studied using dynamic mean-field schemes,[18] as well as dynamic Monte Carlo,[19−25] molecular dynamics,[26−30] and Brownian dynamics[31,32] techniques. Some of the dynamic studies were conducted on single polymers at a surface,[22,25,31] while others comprised adsorption from solution ranging from semidilute conditions[20,19,21,23,24,30,32] to polymer melts.[26−29] Various static and dynamic properties of polymer adsorption have been examined as a function of strength of the polymer−surface interaction,[14,17,21,23,31] and only a few have been conducted on polymer models with varying intrinsic stiffness.[14,16,31] Furthermore, some attention has been given to diffusion and exchange in an adsorbed layer.[21,26,27,23,32]

In our previous work,[31] we investigated the adsorption of *single polymers* in good solvent onto solid surfaces using a

*Corresponding author.

 Published on Web 01/29/2010

coarse-grained model. The transition from bulk to fully relaxed equilibrium structures is a complex process involving three distinct phases comprising different time scales: (i) an initial distortion phase, where the polymer becomes deformed by its weak interaction with the solid surface; (ii) an attachment phase, where the polymer starts to physically attach to the surface and partly spread on it; (iii) a relaxation phase, during which the polymer continues to spread on the surface until it reaches full equilibrium. In our second contribution,[32] adsorption of flexible polymers in good solvent onto a planar and solid surface for different polymer *lengths* and *densities* was examined. When the adsorption takes place from a polymer solution, the situation becomes more complex due to the polymer−polymer interaction between adsorbed polymers. Near the end of the adsorption process, a fourth relaxation phase was identified involving shape and conformational rearrangement of adsorbed polymers and driven by repulsive polymer−polymer interactions.

In this study, we extend our simulation studies on the adsorption of polymers in good solvent onto solid surfaces by systematically considering systems with varying *polymer flexibility* and with varying *polymer−surface interaction strength*. Again, a coarse-grained polymer model examined by using Brownian and Monte Carlo simulations is employed. In particular, we (A) more thoroughly examined the fourth relaxation phase for flexible polymers, and (B) describe another slow relaxation phase of the adsorption of rod-like polymers involving a packing of the polymers into a nematic structure. Furthermore, (C) the integration time required to fully integrate polymers into the adsorbed polymer layer is defined. Integration times and residence times of fully integrated polymers were found to increase with increasing polymer stiffness and increasing bead−surface attraction.

2. Model

Basically, the same model is used as previously described.[31,32] The adsorption of polymers from solution onto a planar surface is studied using a simple coarse-grained model. The solution contains N_p polymers and each polymer is represented by a sequence of N_b spherical beads connected via harmonic potentials. The total number of beads in the system N is thus given by $N = N_pN_b$. The polymers are confined in a rectangular simulation box with the box lengths L_x, L_y, and L_z. At $z = \pm(L_z/2)$ we have adsorbing surfaces, whereas periodic boundary conditions are applied in the x- and y-directions. The length of the box edges are $L_x = L_y = 200$ Å and $L_z = 240$ Å.

Because the two surfaces are equivalent, results are averaged over both of them, and henceforward we refer to events occurring at a single surface. Furthermore, since our focus is on events occurring near the surface, in the following a new coordinate system is adopted, in which the z-axis starts at $z = L_z/2$ with its direction pointing into the solution.

The total potential energy U of the system can be expressed as a sum of four different terms: nonbonded bead−bead potential energy $U_{nonbond}$, bond potential energy U_{bond}, angular potential energy U_{angle}, and a bead−surface potential energy U_{surf}, according to

$$U = U_{nonbond} + U_{bond} + U_{angle} + U_{surf} \tag{1}$$

The nonbonded bead−bead potential energy is assumed to be pairwise additive according to

$$U_{nonbond} = \sum_{i<j}^{N} u(r_{ij}) \tag{2}$$

where the truncated and shifted repulsive Lennard-Jones (LJ) potential energy given by

$$u(r_{ij}) = \begin{cases} 4\varepsilon\left[-\left(\frac{\sigma}{r_{ij}}\right)^6 + \left(\frac{\sigma}{r_{ij}}\right)^{12} + \frac{1}{4}\right], & r_{ij} \le 2^{1/6}\sigma \\ 0, & r_{ij} > 2^{1/6}\sigma \end{cases} \tag{3}$$

is used for the interaction between beads i and j, where r_{ij} is the distance between the two beads, $\sigma = 3.405$ Å the diameter of the bead, and $\varepsilon = 0.9961$ kJ/mol the interaction strength. The truncation and the shift of the Lennard-Jones potential yields a soft repulsive potential.

The bond potential energy is given by

$$U_{bond} = \frac{1}{2}k_{bond}\sum_{p=1}^{N_p}\sum_{i=1}^{N_b-1}(r_{i,p} - r_{eq})^2 \tag{4}$$

where $r_{i,p}$ is the length of the bond between bead i and $i+1$ of the pth polymer, $k_{bond} = 2.4088$ kJ/(mol Å^2), the bond force constant, and $r_{eq} = 5.0$ Å, the equilibrium bond length. Furthermore, the angular potential energy is given by

$$U_{angle} = \frac{1}{2}k_{angle}\sum_{p=1}^{N_p}\sum_{i=2}^{N_b-1}(\theta_{i,p} - \theta_{eq})^2 \tag{5}$$

where $\theta_{i,p}$ is the angle formed by beads $i-1$, i, and $i+1$ of the pth polymer, k_{angle} the angular force constant that determines the stiffness of the polymer, and $\theta_{eq} = 180^\circ$, the equilibrium bond angle. In the presence of all interactions, the root-mean-square (rms) bead−bead separation of bonded beads along the polymers becomes $\langle R_{bb}^2\rangle^{1/2} \approx 5.5$ Å.

The polymer−surface interaction is taken as a sum of bead−surface interactions according to

$$U_{surf} = \sum_{i=1}^{N}(u_{surf}(z_i) + u_{surf}(L_z - z_i)) \tag{6}$$

where an attractive 3−9 LJ potential[33]

$$u_{surf}(z_i) = \frac{2\pi}{3}\rho_s\sigma_s^3\varepsilon_s\left[-\left(\frac{\sigma_s}{z_i}\right)^3 + \frac{2}{15}\left(\frac{\sigma_s}{z_i}\right)^9\right] \tag{7}$$

is used for the interaction between bead i and a surface. In eq 7, ρ_s is the density of the (hypothetical) particles forming the surface, σ_s the mean diameter of a bead and a surface particle, ε_s a potential energy parameter describing the bead−surface interaction, and z_i the z-coordinate of bead i with respect to the surface. For simplicity, $\sigma_s = 3.5$ Å and $\rho_s\sigma_s^3 = 1$ were chosen. With this attractive 3−9 LJ potential, the potential minimum appears at $z_{min} = (2/5)^{1/6}\sigma_s \approx 3.0$ Å and amounts to $u_{surf}(z_{min}) = -[2\pi(10)^{1/2}/9]\rho_s\sigma_s^3\varepsilon_s \approx -2.2\varepsilon_s$.

In this work, $N_p = 1056$ polymers with chain length $N_b = 20$ have been considered at variable (i) flexibility and (ii) bead−surface interaction, regulated by k_{angle} and ε_s, respectively. With the radius of gyration $\langle R_g^2\rangle^{1/2} = 12.50$ Å for flexible 20-mer at infinite dilution,[32] we obtain $(4\pi/3)\langle R_g^2\rangle^{3/2}N_p/(L_xL_yL_z) = 0.9$; thus, the bulk density is near the overlap density.

In our previous work,[32] the dynamic adsorption of 20-mers and of 80-mers at 0.9 times their overlap concentration was examined. Thus, corresponding states of solutions with polymers of different length were considered. The expected faster self-diffusion and end-to-end vector reorientation dynamics of the

Table 1. Model Parameters

box length (x- and y-direction)	$L_x = L_y = 200$ Å
box length (z-direction)	$L_z = 240$ Å
temperature	$T = 298$ K
number of beads in a polymer	$N_b = 20$
number of polymers	$N_p = 1056$
bead−bead LJ parameter	$\sigma = 3.405$ Å
bead−bead LJ parameter	$\varepsilon = 0.9961$ kJ/mol
force constant of bond potential	$k_{bond} = 2.4088$ kJ/(mol Å^2)
equilibrium separation of bond potential	$r_{eq} = 5.0$ Å
force constant of angle potential	k_{angle} = 0,0.3,1.2,3,6,10,20, and 30 J/(mol deg^2)
equilibrium angle of angle potential	$\theta_{eq} = 180^o$
bead−surface LJ parameter	$\sigma_s = 3.5$ Å
bead−surface LJ parameter	ε_s = 1.5,2.0,2.5,3.0, and 3.5 kJ/mol

Table 2. Conversion to Reduced Units

length	$L^* = L/\sigma$
density	$\rho^* = \rho\sigma^3$
interaction energy	$\varepsilon^* = \varepsilon/RT$
force constant of bond potential	$k^*_{bond} = k_{bond}\sigma^2/RT$
force constant of angle potential	$k^*_{angle} = k_{angle}/RT$
time	$t^* = t/(\sigma 2D_0)$

shorter polymer at infinite dilution was found. The adsorption dynamics was an order of magnitude faster for the 20-mers, but no principal differences between the two polymer lengths were detected. (i) The qualitative same behavior and (ii) the faster adsorption dynamics motivated us to use the shorter 20-mer in the present systematic study.

In total 40 systems involving eight different chain flexibilities and five different bead−surface interaction strengths have been examined. The different angular force constants were k_{angle} = 0, 0.3, 1.2, 3, 6, 10, 20, and 30 J/(mol deg^2) ranging from fully *flexible* ($k_{angle} = 0$) over *semiflexible* ($k_{angle} = 1.2$ J/(mol deg^2)) and *stiff* ($k_{angle} = 10$ J/(mol deg^2)) to *rod-like* ($k_{angle} = 30$ J/(mol deg^2)) polymers. The different bead−surface interaction strengths were ε_s = 1.5, 2.0, 2.5, 3.0, and 3.5 kJ/mol ranging from *weak* ($\varepsilon_s = 1.5$ kJ/mol) over *intermediate* ($\varepsilon_s = 2.5$ kJ/mol) to *strong* ($\varepsilon_s = 3.5$ kJ/mol) bead−surface attraction.

Three sets in the (k_{angle}, ε_s)-space will be of particular interest: (i) set I comprising systems characterized by the intermediate bead−surface interaction strength ($\varepsilon_s = 2.5$ kJ/mol) at variable angular force constant k_{angle}, (ii) set II comprising systems with flexible polymers ($k_{angle} = 0$) at variable bead−surface interaction strength ε_s, and (iii) set III comprising systems with rod-like polymers ($k_{angle} = 30$ J/(mol deg^2)) at variable bead−surface interaction strength ε_s. General model parameters are compiled in Table 1, conversions to reduced units in Table 2, and systems investigated and their labeling in Table 3.

The intrinsic flexibility of the polymers was characterized by calculating the persistence length based on the local folding l_p of a single polymer in infinite dilution according to $l_p = \langle R_{bb}{}^2\rangle^{1/2}/(1 + \langle\cos\theta\rangle)$.[34,35] The persistence length of the single polymers with the different angular force constants became l_p = 6.5, 7.8, 13, 26, 47, 77, 149, and 221 Å, respectively. The contour length is $L = (N_b - 1)\langle R_{bb}{}^2\rangle^{1/2} \approx 105$ Å.

3. Methods

3.1. Simulation Details. In this work, both static and dynamic properties of polymer solutions have been examined. Monte Carlo (MC) simulations were used to obtain equilibrium properties, whereas Brownian dynamics (BD) simulations were used to examine the adsorption dynamics

Table 3. Overview of Investigated Systems[a]

	k_{angle} (J/(mol deg^2))							
ε_s (kJ/mol)	0[b]	0.3	1.2[c]	3	6	10[d]	20	30[e]
1.5[f]	II							III
2.0	II							III
2.5[g]	I, II	I	I	I	I	I	I	I, III
3.0	II							III
3.5[h]	II							III

[a] I, II, and III denote that the system belongs to set I, set II, and set III, respectively. [b] Referred to as flexible polymer. [c] Referred to as semiflexible polymer. [d] Referred to as stiff polymer. [e] Referred to as rod-like polymer. [f] Referred to as weak bead−surface attraction. [g] Referred to as intermediate bead−surface attraction. [h] Referred to as strong bead−surface attraction.

and the associated change of the internal structure of the polymers. MC simulations were also used to prepare the initial configurations of the BD simulations. The canonical ensemble (NVT), characterized by a constant number of particles, volume, and temperature was used throughout. The variable adsorption among the systems lead to a variation of the bulk polymer density (density far from the surfaces) up to 10%. Two additional simulations have been made to examine the consequences of 10% variation of the bulk polymer density. All simulations were performed using the integrated Monte Carlo/molecular dynamics/Browninan dynamics simulation package MOLSIM.[36]

In more detail, the MC simulations were performed according to the Metropolis algorithm[37] using three types of trial moves: (i) translation of individual beads, (ii) reptation of polymers, and (iii) translation of polymers. The translational displacement parameter of single-bead trial moves was 3 Å, the probability of a reptation and of a polymer translation was $1/N_b$ of that of a single-bead trial move, and the polymer translational displacement parameter was 5 Å. The MC simulations comprised 1×10^5 trial moves per bead after equilibration.

The dynamic adsorption simulation studies were carried out as follows: (i) First, preparative MC stimulation of polymer solutions confined in a box with hard walls at the edges in the z-direction with $L_z = 200$ Å and periodic boundary conditions in the x- and y-direction were performed. (ii) Second, the hard walls were removed, the box length in the z-direction was increased to $L_z = 240$ Å, and attractive surfaces, whose potential described by eq 7, were invoked. (iii) Finally, the BD simulations were initiated. Hence, the initial configurations of the BD simulations involved a ≈ 20 Å thick polymer-free zone adjacent to each attractive surface. Beads located 20 Å from a surface experience the negligible bead−surface potential $u_{surf} \approx 10^{-3}\, k_bT$, which is only 0.05% of the value at z_{min}; hence, the initial polymer adsorption ought to be controlled by translational diffusion.

The motion of the polymer beads in the BD simulations was described by Ermak[38]

$$\mathbf{r}_i(t+\Delta t) = \mathbf{r}_i(t) + \frac{D_0\Delta t}{k_bT}\mathbf{F}_i(t) + \mathbf{R}_i(t;\Delta t) \qquad (8)$$

where $\mathbf{r}_i(t+\Delta t)$ is the location of bead i at the time $t+\Delta t$, $\mathbf{r}_i(t)$ the location of bead i at the time t, D_0 the bead self-diffusion coefficient in the absence of systematic forces, k_b Boltzmann's constant, T the temperature, and $\mathbf{F}_i(t)$ the systematic force on bead i at time t arising from the potential energy U given by eq 1. Furthermore, $\mathbf{R}_i(t;\Delta t)$ is a random displacement of bead i representing the effect of collisions with solvent molecules at time t and is sampled from a Gaussian

distribution with the mean $\langle \mathbf{R}_i(t;\Delta t)\rangle = 0$ and the variance $\langle \mathbf{R}_i(t;\Delta t) \cdot \mathbf{R}_j(t';\Delta t)\rangle = 6D_0\Delta t\delta_{ij}\delta(t-t')$ as obtained from the fluctuation−dissipation theorem. In this work, hydrodynamic interactions were neglected.

A bead self-diffusion coefficient $D_0 = 0.1$ Å^2/ps was used, and an integration time step $\Delta t = 0.025$ ps was employed. The BD simulations involved 3.2×10^7 time steps, providing a nominal simulation time of 800 ns. Using $\tau_{BD} = \sigma^2/D_0 = 116$ ps as the conventional unit of time, the integration time step becomes $\Delta t = 2.2 \times 10^{-4}\ \tau_{BD}$ and the total simulation time $6.9 \times 10^3\ \tau_{BD}$. For a single flexible polymer with 20 beads in an infinite dilute solution, previous investigation[31] gave the polymer self-diffusion coefficient $D = 0.005$ Å^2/ps and the relaxation time $\tau_R = 55$ ns characterizing the end-to-end vector time correlation function.

The statistical uncertainties of the equilibrium properties given in figures and based on block averaging are negligible, whereas those of dynamic properties are comparable to symbol size unless otherwise is stated.

3.2. Analysis. A bead is considered as being adsorbed if it is in contact with the surface, here defined by $z_i < z_{ads} \equiv 6$ Å, and a polymer is considered as being adsorbed if at least one of its beads is adsorbed. The bead−surface potential energy at $z = z_{ads}$ is $u_{surf}(z_{ads}) = -0.41\varepsilon_s$, thus ranging from $-0.25k_bT$ at $\varepsilon_s = 1.5$ kJ/mol to $-0.58k_bT$ at $\varepsilon_s = 3.5$ kJ/mol. Also, recall that the minimum of the bead−surface potential is located at $z_{min} \approx 3$ Å. Both the average number of adsorbed beads $\langle N_b^{ads}\rangle$ and of adsorbed polymers $\langle N_p^{ads}\rangle$ onto the *two* surfaces as well as their time dependences $N_b^{ads}(t)$ and $N_p^{ads}(t)$ will be exmined. Furthermore, the same distance threshold z_{ads} is used to define adsorbed bonds, now applied to the center of a bond. The criteria for when a bead or a bond is considered adsorbed is somewhat arbitrary. The value of the adsorption threshold z_{ads} will generally influence the numbers obtained but not qualitative aspects.

The location of a polymer was described using its center-of-mass (com) $\mathbf{r}_{com}$ defined according to

$$\mathbf{r}_{com} = \frac{1}{N_b}\sum_{i=1}^{N_b}\mathbf{r}_i \tag{9}$$

where $\mathbf{r}_i = (x_i,y_i,z_i)$ is the coordinate of bead i at time t. Changing the notation $\mathbf{r}_i$ to z_i in eq 9 gives the com along the z-axis, z_{com}, which is a useful measure of the position of the polymers relative to the surface.

The extension of a polymer in three dimensions is given by its rms radius of gyration, R_g, defined according to

$$R_g^{\,2} = \frac{1}{N_b}\sum_{i=1}^{N_b}(\mathbf{r}_i - \mathbf{r}_{com})^2 \tag{10}$$

There is a structural rearrangement of the polymers during the adsorption and a preferential orientation with respect to the surface. This rearrangement was followed by studying the perpendicular ($\perp$) and parallel ($\parallel$) component of R_g according to

$$R_{g\perp}^{\,2} = \frac{1}{N_b}\sum_{i=1}^{N_b}(z_i - z_{com})^2 \tag{11}$$

$$R_{g\parallel}^{\,2} = \frac{1}{N_b}\sum_{i=1}^{N_b}[(x_i - x_{com})^2 + (y_i - y_{com})^2] \tag{12}$$

satisfying $R_g^{\,2} = R_{g\perp}^{\,2} + R_{g\parallel}^{\,2}$.

The structure of adsorbed polymers was described by using tail, loop, and train subchains.[7] A subchain of adsorbed beads is referred to as a train, a nonadsorbed subchain with both ends bonded to trains as a loop, and a nonadsorbed subchain with one end bonded to a train as a tail. The total number of beads in subchains of type α at time t will be denoted by N_α with $\alpha = \{\text{tail, loop, train}\}$. By conservation: $\Sigma_\alpha N_\alpha = N_b$. Both equilibrium values $\langle N_\alpha\rangle$ and time-dependent values $N_\alpha(t)$ averaged over adsorbed polymers will be presented. Finally, $\langle N_{tail}\rangle = \langle N_b^{ads}\rangle/\langle N_p^{ads}\rangle$.

The degree of nematic order appearing in the adsorbed polymer layer was examined by considering the bond order parameter η. The degree of bond order in the neighborhood of the adsorbed bond i, η_i, was evaluated as

$$\eta_i = \lambda_i^+ \tag{13}$$

where λ_i^+ is the largest eigenvalue of the 3×3 matrix $\mathbf{B}_i$, which elements are defined by

$$\mathbf{B}_{\alpha\beta,\,i} = \frac{1}{N_{V_i}}\sum_{j\in V_i}\frac{1}{2}(3\mathbf{b}_{\alpha,j}\mathbf{b}_{\beta,j} - \delta_{\alpha\beta}) \tag{14}$$

with $\mathbf{b}_{\alpha,j}$,$\alpha = \{x,y,z\}$, being the projection of the normalized bond vector $\mathbf{b}_j$ of bond j on the α-axis and $\delta_{\alpha\beta}$,$\{\alpha,\beta\} = \{x,y,z\}$, the Kronecker delta and where the summation involves N_{Vi} bonds in the spherical volume V_i with the radius R_η centered at bond i. The radii $R_\eta = 10$, 20, and 50 Å have been used, of which results are given for $R_\eta = 20$ Å. Only bonds j that are adsorbed are included in the sum; thus, in practice bonds in a disk of radius R_η and thickness 3 Å are included. The bond order parameter ranges from zero for random bond directions to unity for completely parallel bond directions. Average equilibrium bond order $\langle\eta\rangle$ and time-dependent bond order $\eta(t)$ will be presented.

Many time-dependent properties are given on a logarithmic time scale to encompass the large dynamic range of the different adsorption subprocesses. These properties were sampled at an interval of $\Delta t_{samp} = 1.0$ ps (40 time steps) and averaged over blocks with an exponentially increasing length with the initial block length being $100\Delta t_{samp} = 0.1$ ns (4000 time steps) and using 1.1 as multiplicative factor of the block length increase.

Adsorption kinetics were evaluated using configurations separated by $100\Delta t_{samp}$. Thus, adsorption and desorption events appearing on a shorter time scale than 0.1 ns are not resolved. Assuming Rouse diffusion, the root-mean-square displacement of a polymer in one dimension becomes 1 Å during this time separation. A smaller time separation than 0.1 ns would lead to a larger number of short-lived adsorbed and desorbed states originating from local chain motion, and a larger time separation to possibly interesting adsorbed and desorbed states becoming undetected.

4. Results

4.1. Equilibrium Properties. *4.1.1. Density Distributions.* The z-distribution of the reduced bead density $\rho_b^*(z)$ and of the reduced com density of polymers $\rho_{com}^*(z)$ near the surface are displayed in Figure 1 for set I (panels a and b), set II (panels c and d), and set III (panels e and f). The bead density distributions given in panels a, c, and e show that up to two layers of beads can appear with the location of the first maximum occurring at $z \approx z_{min}$ and the second maximum about 4 Å further away from the surface. The geometrical adsorption threshold z_{ads} falls approximately between the first and second peak of the bead density. Panels b, d, and f

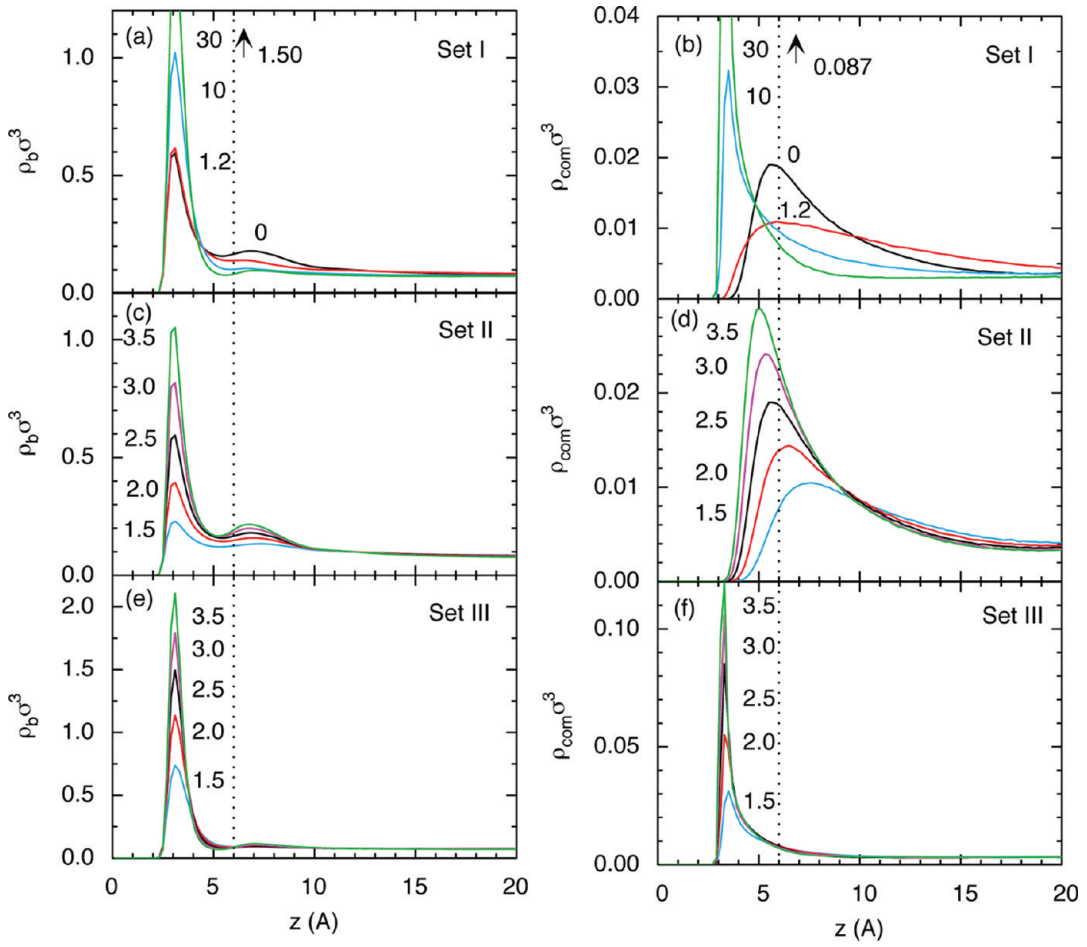

Figure 1. (a, c, and e) Reduced bead density $\rho_b^*(z) = \rho_b(z)\sigma^3$ and (b, d, and f) reduced polymer density $\rho_{com}^*(z) = \rho_{com}(z)\sigma^3$ as a function of z-coordinate near a surface for (a, b) $\varepsilon_s = 2.5$ kJ/mol (intermediate bead−surface interaction strength) at indicated values of k_{angle} in J/(mol deg^2) (set I), (c, d) $k_{angle} = 0$ (flexible polymers) at indicated values of ε_s in kJ/mol (set II), and (e, f) $k_{angle} = 30$ J/(mol deg^2) (rod-like polymers) at indicated values of ε_s in kJ/mol (set III). The values at the arrows denote the hight of the maximum for the system with $k_{angle} = 30$ J/(mol deg^2). The location of the adsorption threshold is also given (dotted vertical lines).

show that the com density distributions display a single maximum near the surface; however, both the locations and the values vary noticeable upon the conditions examined here.

In more detail, at increasing polymer stiffness in set I (Figure 1a) the bead density in the first layer is initially constant but then increases, whereas the bead density in the second layer decreases and vanishes for sufficiently stiff polymers. For the rod-like polymer a weak depletion is found outside the first layer. For flexible polymers in set II (Figure 1c), a very weak maximum appears at the smallest bead−surface interaction strength and the density of both layers increases simultaneously at increasing bead−surface interaction strength. As to the rod-like polymers in set III (Figure 1e), the magnitude of the first layer increases at increasing bead−surface interaction strength, and only a hint of a second layers appears at the strongest interaction strength.

The density distribution of the com displays an interesting behavior at increasing polymer stiffness in set I (Figure 1b). The maximum for flexible polymers appears at $z \approx 6$ Å. For semiflexible polymers, the magnitude of the maximum decreases and the maximum broadens toward the surface and the bulk. Regarding the stiff and rod-like polymers, the maximum of the com distribution shifts to $z \approx 3.3$ Å with decreased width and amplified magnitude with increasing stiffness. At increasing interaction strength (Figure 1d), the maximum of the com density distribution is increased and shifted toward the surface in a continuous manner for flexible polymers, whereas for rod-like polymers (Figure 1f) the maximum of the com density distribution is increased at essentially equal distance from the surface.

In summary, the bead−surface attraction gives rise to adsorbed polymer layers encompassing at most two distinct bead layers and extending at most 10 Å from the surface, whereas the single peak of the com density distribution often is broader. At increasing bead−surface interaction strength (set II and set III), the bead and com density distributions display a regular increasing behavior; i.e., the density maxima appearing at higher interaction strengths are more prominent. However, and as we will encounter below, at increasing polymer stiffness (set I) the situation normally becomes nonmonotonic: here, manifesting that at increasing stiffness (i) the bead density of the first layer increases but the density of the second layer decreases and (ii) a nonmonotonic variation of the amplitude of the single maximum of the com density distribution.

4.1.2. Adsorbed Amount. The average number of adsorbed beads $\langle N_b^{ads} \rangle$ and of adsorbed polymers $\langle N_p^{ads} \rangle$ at the surface are given in Figure 2. Generally, the variation of the average number adsorbed *beads* is stronger (nearly 4-fold) as compared to the variation of the average number of adsorbed *polymers* (less than 2-fold) across the variation of polymer flexibility and bead−surface interaction strength.

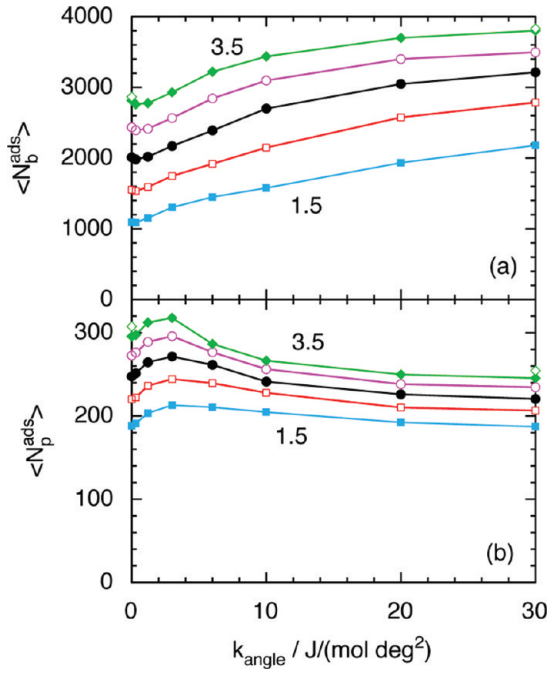

Figure 2. (a) Average number of adsorbed beads $\langle N_b^{ads}\rangle$ and (b) average number of adsorbed polymers $\langle N_p^{ads}\rangle$ as a function of the angular force constant k_{angle} at ε_s = 1.5, 2.0, 2.5, 3.0, and 3.5 kJ/mol. Corresponding results for k_{angle} = 0 and 30 J/(mol deg^2) at ε_s = 3.5 kJ/mol with a 10% larger bulk density are also given (open diamonds).

First, both $\langle N_b^{ads}\rangle$ and $\langle N_p^{ads}\rangle$ display monotonic increases at increasing bead−surface interaction strength for all polymer stiffnesses. Of more interest is the dependence on the polymer flexibility. The average number of adsorbed beads increases with polymer stiffness by 100% at the weakest and by 25% at the strongest bead−surface interaction strength (Figure 2a). However, a small decrease in $\langle N_b^{ads}\rangle$ is observed for slightly nonflexible polymers. The number of adsorbed polymers shows a richer behavior, displaying a prominent increase as initially flexible polymers become semiflexible and thereafter a decrease as the polymers become even stiffer (Figure 2b). The magnitude of the rise at increasing polymer stiffness is similar at the different bead−surface interaction strengths, whereas the decrease after the maximum becomes more pronounced with growing interaction strength. The location of the maximum of $\langle N_p^{ads}\rangle$ shifts to lower stiffness with increasing interaction strength, and the maxima appears at persistence lengths of l_p = 20−30 Å.

As alluded to above, the larger adsorption at higher ε_s implies that the polymer bulk density decreases at increasing ε_s. The bulk density for ε_s = 3.5 kJ/mol becomes ≈10% lower than for ε_s = 1.5 kJ/mol. Figure 2 also show results for k_{angle} = 0 and 30 J/(mol deg^2) and ε_s = 3.5 kJ/mol with a 10% enhanced bulk density (open diamonds), hence having the same bulk density as for ε_s = 1.5 kJ/mol. As can be seen, neither $\langle N_b^{ads}\rangle$ nor $\langle N_p^{ads}\rangle$ are significantly affected by a 10% variation of the bulk density, signifying that we are on the plateau of the adsorption isotherm. In the following, we will neglect the small bulk density variation among the systems and the even smaller influence on the equilibrium properties of the adsorbed polymer layer.

We conclude that (i) a slight increase in the polymer stiffness of initially flexible polymers leaves the number of adsorbed beads fairly constant but promotes the number of adsorbed polymers, whereas (ii) a further increase in polymer stiffness increases the number of adsorbed beads and decreases the number of adsorbed polymers. The resulting variation of the fraction of adsorbed beads of an adsorbed polymer $\langle N_b^{ads}\rangle/\langle N_p^{ads}\rangle$ implies that adsorbed polymers of different flexibility possess different conformations.

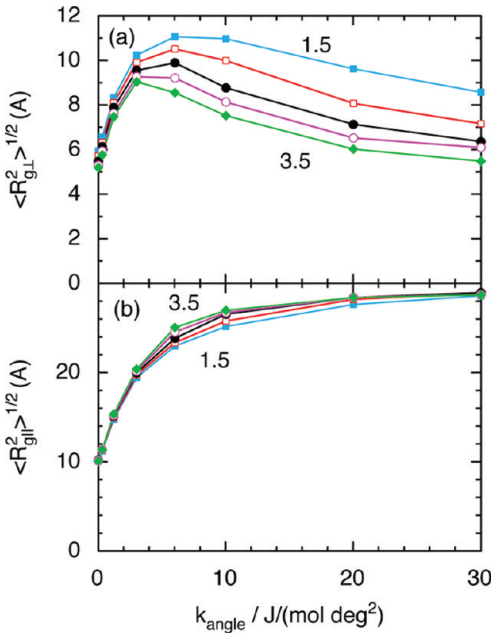

Figure 3. (a) Perpendicular component of the rms radius of gyration $\langle R_{g\perp}^2\rangle^{1/2}$ and (b) parallel component of rms radius of gyration $\langle R_{g\parallel}^2\rangle^{1/2}$ of adsorbed polymers as a function of the angular force constant k_{angle} at ε_s = 1.5, 2.0, 2.5, 3.0, and 3.5 kJ/mol.

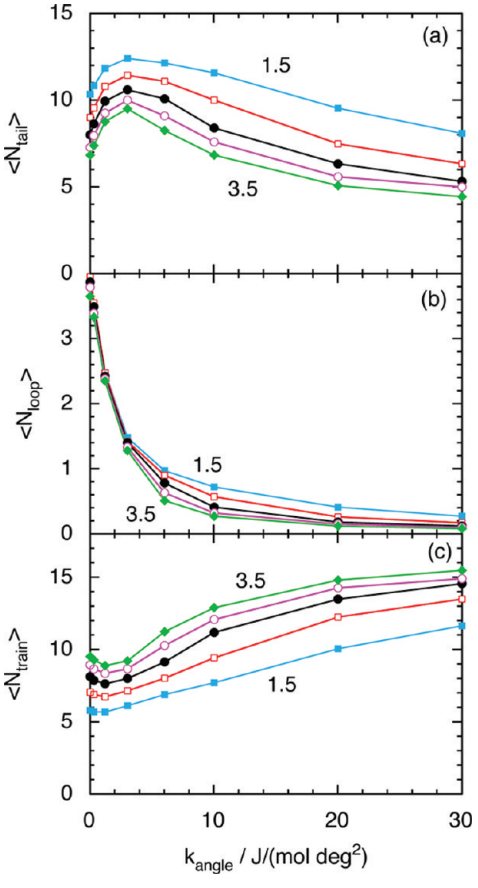

Figure 4. Average number of beads residing in (a) tails $\langle N_{tail}\rangle$, (b) loops $\langle N_{loop}\rangle$, and (c) trains $\langle N_{train}\rangle$ of adsorbed polymers as a function of the angular force constant k_{angle} at ε_s = 1.5, 2.0, 2.5, 3.0, and 3.5 kJ/mol.

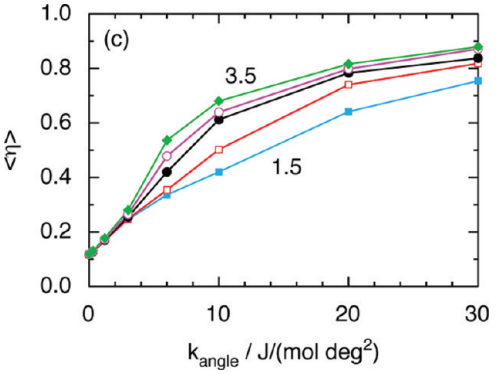

Figure 5. Average bond order $\langle\eta\rangle$ as a function of the angular force constant k_{angle} at R_η = 20 Å and at ε_s = 1.5, 2.0, 2.5, 3.0, and 3.5 kJ/mol.

4.1.3. Structural Properties. In this subsection, we will focus on structural properties of adsorbed polymers. Normalized probability functions of the perpendicular $P(R_{g\perp})$ and parallel $P(R_{g\parallel})$ component of the radius of gyration of flexible, semiflexible, stiff, and rod-like polymers at the intermediate bead−surface interaction strength (set I) have been extracted. From these results (data not shown), we find that adsorbed flexible and semiflexible polymers become stretched parallel to the surface and contracted perpendicular to the surface. As to stiff and rod-like polymers, most polymers have their long-axes oriented parallel to the surface; however, extended tails of $P(R_{g\perp})$ and $P(R_{g\parallel})$ demonstrate that some polymers still protrude away from the surface.

The two components of the radius of gyration as a function of k_{angle} at various bead−surface interaction strength are shown in Figure 3. We find that $\langle R_{g\perp}{}^2\rangle^{1/2}$ first increases, reaches a maximum, and is then reduced at increasing polymer stiffness (Figure 3a). The locations of the maxima are shifted to higher flexibility at increasing bead−surface interaction strength. The locations of the maxima display the same trend as those for the average number of adsorbed polymers shown in Figure 2b. Thus, the nonmonotonic dependence of average number of adsorbed polymers $\langle N_p^{ads}\rangle$ and of the perpedicular component of the rms radius of gyration $\langle R_{g\perp}{}^2\rangle^{1/2}$ ought to be related. Furthermore, $\langle R_{g\parallel}{}^2\rangle^{1/2}$ (Figure 3b) increases continuously with increasing polymer stiffness, and increases somewhat with increasing bead−surface interaction at intermediate polymer flexibility.

We will now consider some results of the tails, loops, and trains characterization. Figure 4 displays the average number of beads residing in tails, loops, and trains as a function of k_{angle} at various bead−surface interaction strengths. Throughout, the average number of beads in tails decreases (Figure 4a) and the number in trains increases (Figure 4c) with increasing bead−surface interaction strength. Moreover, the average number of beads in loops is only weakly dependent on the bead−surface interaction strength at small and at large angular force constants and decreases substantially at intermediate angular force constant (Figure 4b). Thus, as expected, the propensity for beads residing in tails decreases, while it increases for trains with increasing surface attraction. This variation depends mainly on the change in the average number of beads in a subchain rather than the change in the average number of subchains (data not shown).

Furthermore, the average number of beads in tails displays a maximum at intermediate polymer stiffness in a similar manner as the perpendicular component of the rms radius of gyration, suggesting that the main contribution to $\langle R_{g\perp}{}^2\rangle^{1/2}$ comes from beads residing in tails. The average number of beads in loops is ≈4 for flexible polymers and reduces to a few tens for rod-like polymers. Obviously, the appearance of loops is not possible for a true rod. The average number of beads residing in trains attains a minimum at small polymer stiffness and a global maximum appears for rod-like polymers where 50−75% of the beads of an adsorbed polymer appears in trains.

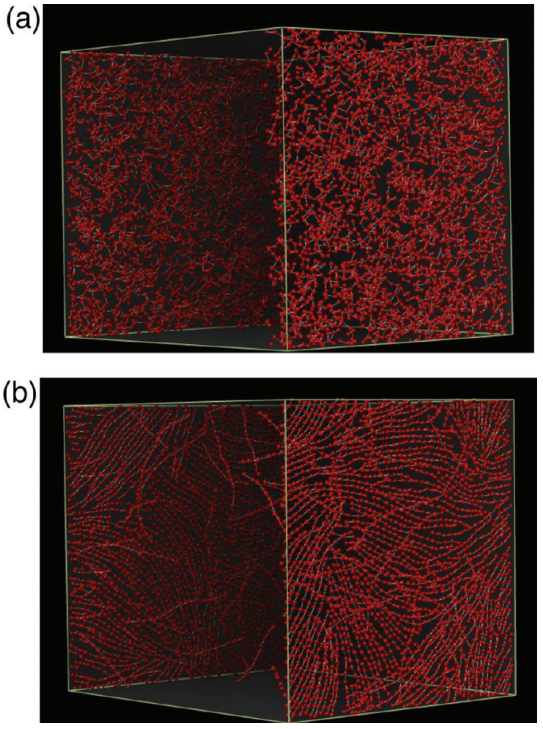

Figure 6. Snapshots displaying adsorbed polymers for (a) k_{angle} = 0 (flexible polymers) and (b) k_{angle} = 30 J/(mol deg²) (rod-like polymers) at ε_s = 3.5 kJ/mol (set I).

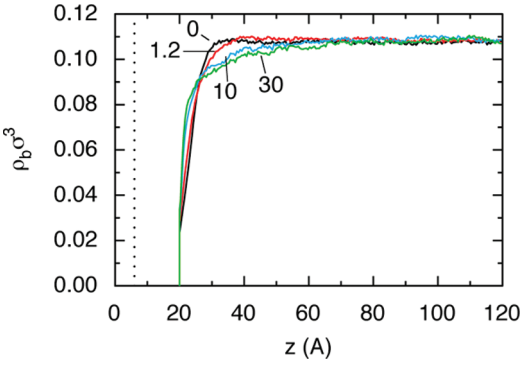

Figure 7. Reduced bead density $\rho_b^*(z) = \rho_b(z)\sigma^3$ of the preparative MC simulation taken as initial bead distribution of the BD simulations at indicated values of k_{angle} in J/(mol deg²) (see text for details). The location of the adsorption threshold is also given (dotted vertical line).

As the polymer is made stiffer, the tendency of a local nematic order of bonds in the adsorbed polymer layer increases. Figure 5 shows the average bond order $\langle\eta\rangle$ at R_η = 20 Å as a function of k_{angle} at all bead−surface interactions strengths. First, the bond order data show virtually no order at all for adsorbed flexible polymers, whereas there is a large order for adsorbed rod-like polymers. For flexible and rod-like polymers, the bond order of adsorbed bonds is insensitive to the bead−surface attraction, however, at intermediate polymer flexibility the bond order increases with increasing

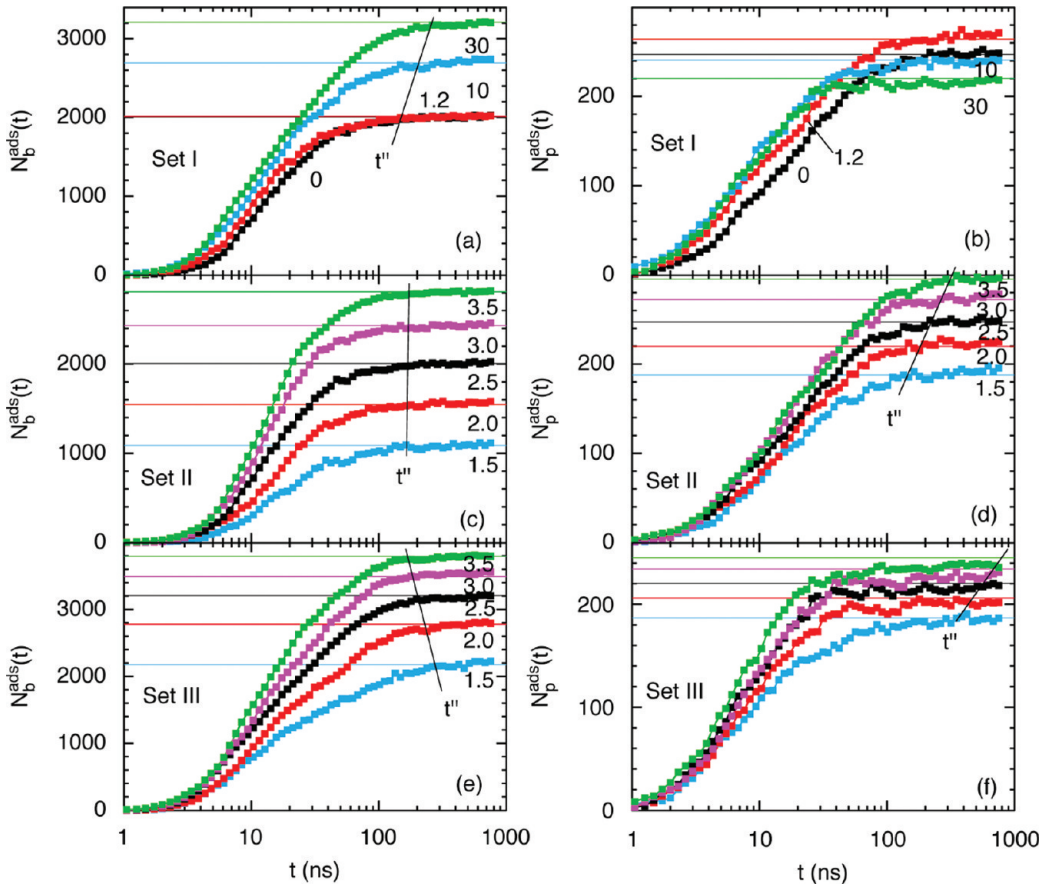

Figure 8. (a, c, and e) Number of adsorbed beads $N_b^{ads}(t)$ and (b, d, and f) number of adsorbed polymers $N_p^{ads}(t)$ as a function of time t on a logarithmic scale for (a, b) $\varepsilon_s = 2.5$ kJ/mol (intermediate bead−surface intermediate strength) at indicated values of k_{angle} in J/(mol deg^2) (set I), (c, d) $k_{angle} = 0$ (flexible polymers) at indicated values of ε_s in kJ/mol (set II), and (e, f) $k_{angle} = 30$ J/(mol deg^2) (rod-like polymers) at indicated values of ε_s in kJ/mol (set III). Equilibrium values obtained from MC simulations are also given (horizontal lines), and the variation of the relaxation times t'' is also indicated (black solid lines).

bead−surface attraction. Thus, the bond order displays a large dependence on the polymer stiffness and less on the bead−surface interaction strength.

Snapshots of final configurations of the MC simulations, for adsorbed flexible and rod-like polymers, are given in Figure 6 and illustrate a number of properties previously quantified. In particular, the change from a disordered to a nematic-like order at increasing polymer stiffness quantified in Figure 5 is obvious. As to the rod-like polymers, it is obvious that some polymers strongly protrude into the solution, giving rise to the tails in $P(R_{g\perp})$ and $P(R_{g\parallel})$ discussed above. Similar observations of "hairpins" extending into solution for adsorbed semiflexible polymers in good solvent have previously been discussed by Kramarenko et al.[14] Noticeable is also the spatial variation of the nematic director across the surfaces.

4.2. Dynamic Properties. As previously mentioned, before the BD simulations preparative MC simulations of polymer solutions were made in a cubic box with $L_z = 200$ Å and hard walls in the z-directions. The reduced equilibrium bead density distribution for polymers with different stiffnesses of the preparative simulations are shown in Figure 7. Since the length in the z-direction was extended at each side by 20 Å prior to the BD simulations, an ≈20 Å thick polymer-free zone adjacent to each adsorbing surface is present at $t = 0$ of the BD simulations. Furthermore, next to this zone there is a steep but gradual increase of the bead density extending about a radius of gyration (10 Å for the flexible to 50 Å for the rod-like polymer) before the bead density attains the bulk value $\rho_b^* \approx 0.107$. This gradual increase is due to a depletion occurring in the vicinity of the hard walls in the preparative simulations.

In the BD simulation, the polymers diffuse to the surface, become physically attached, and undergo various structural relaxation processes. In the following, t' will denote the time of the onset of the first polymer attachment and t'' the time at which a quantity has relaxed to its equilibrium value. As we will see, t'' is generally property dependent. The equilibrium values given below are taken from the separate MC simulations. Generally, there is perfect agreement between the equilibrium values obtained from the MC simulations and the values of the corresponding properties at the end of the BD simulations. The only exception appears for some properties of systems containing rod-like polymers, which display very slow relaxation.

4.2.1. Adsorbed Amount. The adsorption process will first be characterized by considering the time dependence of the number of adsorbed beads and of the number of adsorbed polymers. The left and right columns of Figure 8 show $N_b^{ads}(t)$ and $N_p^{ads}(t)$, respectively, as a function of the simulation time t in a logarithmic representation for systems belonging to set I (top row), set II (middle row), and set III (bottom row). Corresponding equilibrium values given in Figure 2 are also shown (horizontal lines) along with the locations of t'' (black solid lines).

Generally, the first polymer becomes adsorbed at $t' \approx 1$ ns. The dependence of the polymer stiffness and the bead−surface interaction strength on t' is weak, particularly in

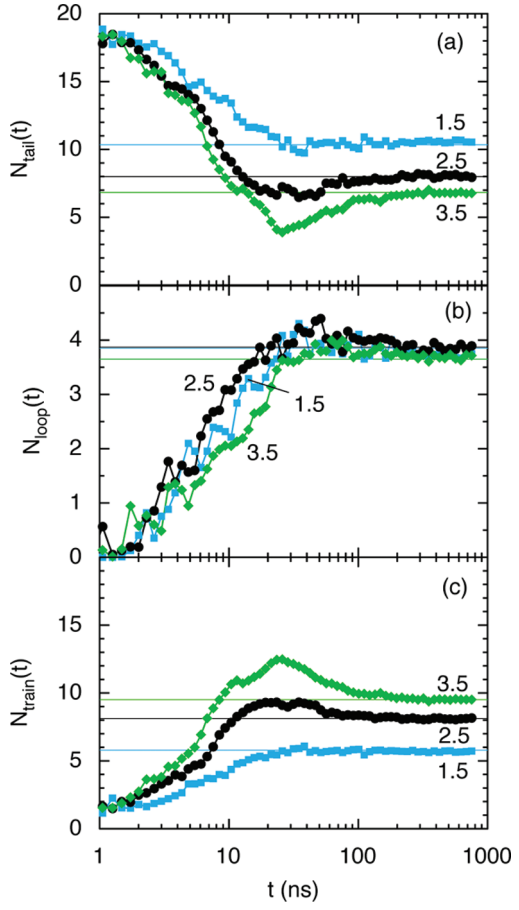

Figure 9. Number of beads residing in (a) tails $N_{tail}(t)$, (b) loops $N_{loop}(t)$, and (c) trains $N_{train}(t)$ of adsorbed polymers as a function of time t on a logarithmic scale for $k_{angle} = 0$ (flexible polymers) at indicated values of ε_s in kJ/mol (set II). Equilibrium values obtained from MC simulations are also given (horizontal lines).

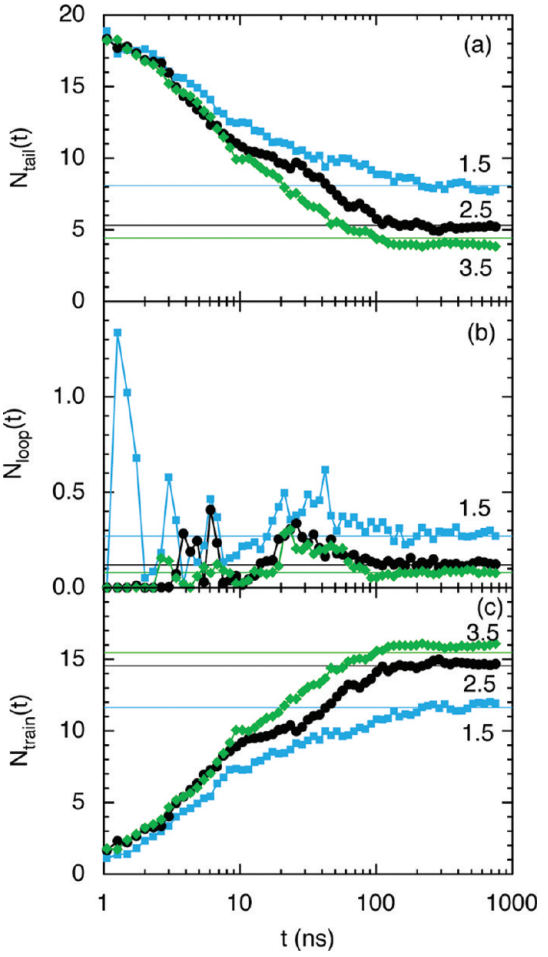

Figure 10. Number of beads residing in (a) tails $N_{tail}(t)$, (b) loops $N_{loop}(t)$, and (c) trains $N_{train}(t)$ of adsorbed polymers as a function of time t on a logarithmic scale for $k_{angle} = 30$ J/(mol deg^2) (rod-like polymers) at indicated values of ε_s in kJ/mol (set III). Equilibrium values obtained from MC simulations are also given (horizontal lines).

comparison to the large dependence of polymer density and of polymer length previously observed (cf. Figure 2b of ref 32). There, for flexible polymers at the intermediate bead−surface interaction strength it was found that (i) a 4-fold decrease of the polymer density or (ii) a 4-fold increase of the polymer length raised t' roughly 10-fold. In the present case, the appearance of a common onset time $t' \approx 1$ ns shows that (i) the initial part of the adsorption is diffusion controlled without any significant drift contribution from the bead−surface attraction and (ii) the concentration diffusion is at most marginally affected by the polymer stiffness at the conditions of this study. The relaxation times t'' of $N_b^{ads}(t)$ and $N_p^{ads}(t)$ are generally system dependent and different; concisely $t' \approx 200$ ns for $N_b^{ads}(t)$ and $t'' \geq 200$ ns for $N_p^{ads}(t)$.

In more detail, $N_b^{ads}(t)$ shows that systems belonging to set I (common bead−surface interaction strength) display an initially faster adsorption at increasing polymer stiffness, and a 2-fold increase of the relaxation time t'' when making flexible polymers rod-like (Figure 8a). The number of adsorbed polymers also shows that the adsorption, with the exception of the final relaxation, becomes faster at increasing polymer stiffness (Figure 8b). Furthermore, for the stiff and rod-like polymers a kink appears at $\tilde{N}_p^{ads}(t) \equiv N_p^{ads}(t)/\langle N_p^{ads} \rangle \approx 0.95$, signaling an onset of a slower relaxation mechanism. The corresponding data for systems belonging to set II (flexible polymers) are given in panels c and d. We find that the characteristic sigmoidal shape is relatively unaffected by a variation of the bead−surface interaction strength. Since the relaxation time t'' of $N_b^{ads}(t)$ is constant and $\langle N_b^{ads} \rangle$ increases, we have an increasing adsorption rate at increasing interaction strength. Moreover, $N_p^{ads}(t)$ also increases with increasing interaction strength, and the associated relaxation time t'' varies, indicating a structural relaxation mechanism that is dependent on the bead−surface interaction strength. Finally, the corresponding data for systems belonging to set III (rod-like polymers) are given in panels e and f. Also here the sigmoidal shape of $N_b^{ads}(t)$ remains, and the appearance of a kink in $N_p^{ads}(t)$ at $\tilde{N}_p^{ads}(t) \approx 0.95$ becomes more prominent at increasing bead−surface interaction strength. The relaxation of $N_b^{ads}(t)$ becomes *faster* (decreasing t'') and the relaxation of $N_p^{ads}(t)$ becomes *slower* (increasing t'') at increasing ε_s. Noticeably, at $\varepsilon_s = 3.5$ kJ/mol (i) we have $\tilde{N}_p^{ads}(t) \approx 0.97 < 1$ at the end of the simulation and (ii) the relaxation of $N_p^{ads}(t)$ is at least 10-fold slower than the relaxation of $N_b^{ads}(t)$, indicating another slow relaxation mechanism than that for flexible polymers.

The effect of a 10% variation of the bulk concentration on $N_b^{ads}(t)$ and $N_p^{ads}(t)$ for the two systems characterized by $k_{angle} = 0$ and 30 J/(mol deg^2) with $\varepsilon_s = 3.5$ kJ/mol has also been considered. A 10% larger bulk concentration leads to 10−20% faster adsorption dynamics, in line with our previous results that a 4-fold reduction of the bulk density reduced the adsorption dynamics by 1 order of magnitude.[32] As for the static equilibrium results, the observed

dependence on the bulk density variation does not significantly affect our conclusions regarding the adsorption dynamics.

Thus, the examination of $N_b^{ads}(t)$ and $N_p^{ads}(t)$ and their variation among the different systems suggests that the slowest relaxation mechanism becomes slower at increasing bead−surface interaction strength[21] and is qualitatively different for flexible and rod-like polymers.

4.2.2. Structural Properties. We will now focus on structural properties characterizing the adsorption, including an examination of the slow relaxation processes alluded to in the previous subsection. The time dependence of the number of beads residing in tails, loops, and trains of three systems belonging to set II (flexible polymers) are shown in Figure 9. The following time dependences are seen: (i) At $t \approx t'$, at which only a few polymers just have been adsorbed, $N_{tail} \approx 18$; thus, nearly all beads in these polymers reside in tails. (ii) Thereafter, the number of beads in tails is reduced and the number of beads in loops and trains increases, demonstrating a structural relaxation of the initially adsorbed polymers as well as of later adsorbed polymers. The initial conformational relaxation is faster for systems with stronger bead−surfce attraction, since in these systems the beads are more strongly drawn toward the surface. (iii.a) As to the system with the weakest bead−surface attraction, ε_s = 1.5 kJ/mol, the number of beads in the various subchains smoothly approaches their equilibrium values at $t \approx 30$ ns, which is faster than the relaxation of the number of adsorbed beads. Thus, here the conformational relaxation is faster than the relaxation of $N_b^{ads}(t)$. (iii.b) For systems with ε_s = 2.5 kJ/mol and even so for ε_s = 3.5 kJ/mol, $N_{tail}(t)$ displays a minimum and $N_{train}(t)$ a maximum at $t \approx 30$ ns whereafter they attain their equilibrium values at $t \approx 200$ ns $\approx t''$. A similar variation of $R_{g\perp}(t)$ and $R_{g\parallel}(t)$ involving an initial relaxation, appearance of extreme values at $t \approx 30$ ns, and a slow relaxation toward their equilibrium values are found (data not shown). Thus, after the polymers have attained an extended shape parallel to the surface, they become laterally compressed, resulting in fewer anchoring points (smaller N_{train}) and longer tails (larger N_{tail}). Since this structural relaxation is completed after $N_p^{ads}(t)$ has relaxed, the structural relaxation ought to be driven by the relaxation of the number of adsorbed polymers $N_p^{ads}(t)$.

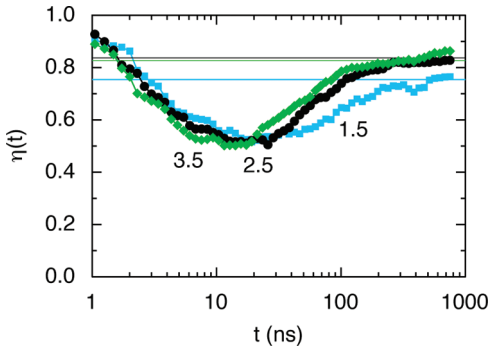

Figure 11. Bond order $\eta(t)$ as a function of time t on a logarithmic scale for k_{angle} = 30 J/(mol deg^2) (rod-like polymers) at R_η = 20 Å and at indicated values of ε_s in kJ/mol (set III). Equilibrium values obtained from MC simulations are also given (horizontal lines).

Figure 10 shows the corresponding time dependence of the number of beads residing in tails, loops, and trains for systems containing rod-like polymers (set III). Also here, there is an initial decrease in $N_{tail}(t)$ and increase in $N_{train}(t)$, whereas $N_{loop}(t)$ is very small ($\ll$1) and displays a large relative uncertainty. Both $N_{tail}(t)$ and $N_{train}(t)$ relax (i) essentially monotonically toward their equilibrium values (ii) on a time scale of $t \approx 100-200$ ns. Also here the relaxation rates increase with increasing bead−surface interaction strength. Furthermore, with the weakest bead−surface interaction strength the monotonic relaxation is 10-fold slower

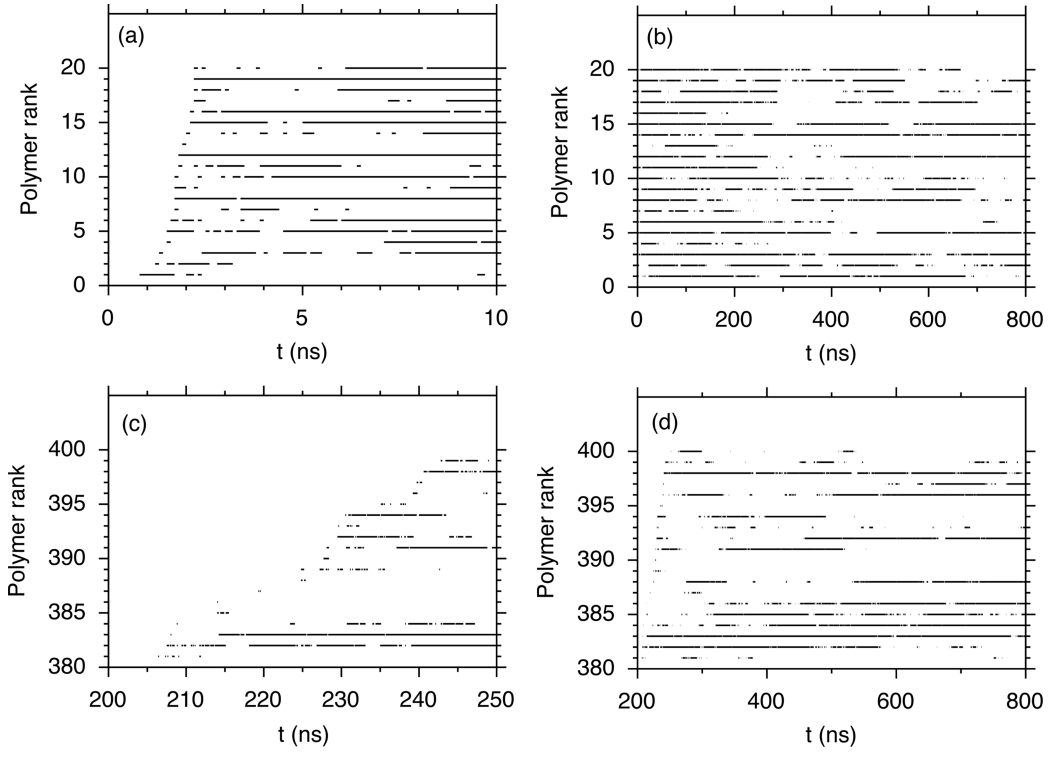

Figure 12. Adsorption history of polymers with different rank where an adsorbed state is represented by a horizontal line as as a function of simulation time of (a and b) the 20 first adsorbed polymers and (c and d) 20 polymers adsorbing after $t \approx 200$ ns for system with k_{angle} = 0 (flexible polymers) at ε_s = 1.5 kJ/mol. The abscissa scale is (a) 10 ns, (b) 800 ns, (c) 50 ns, and (d) 600 ns. Adsorption and desorption time resolution is 0.1 ns.

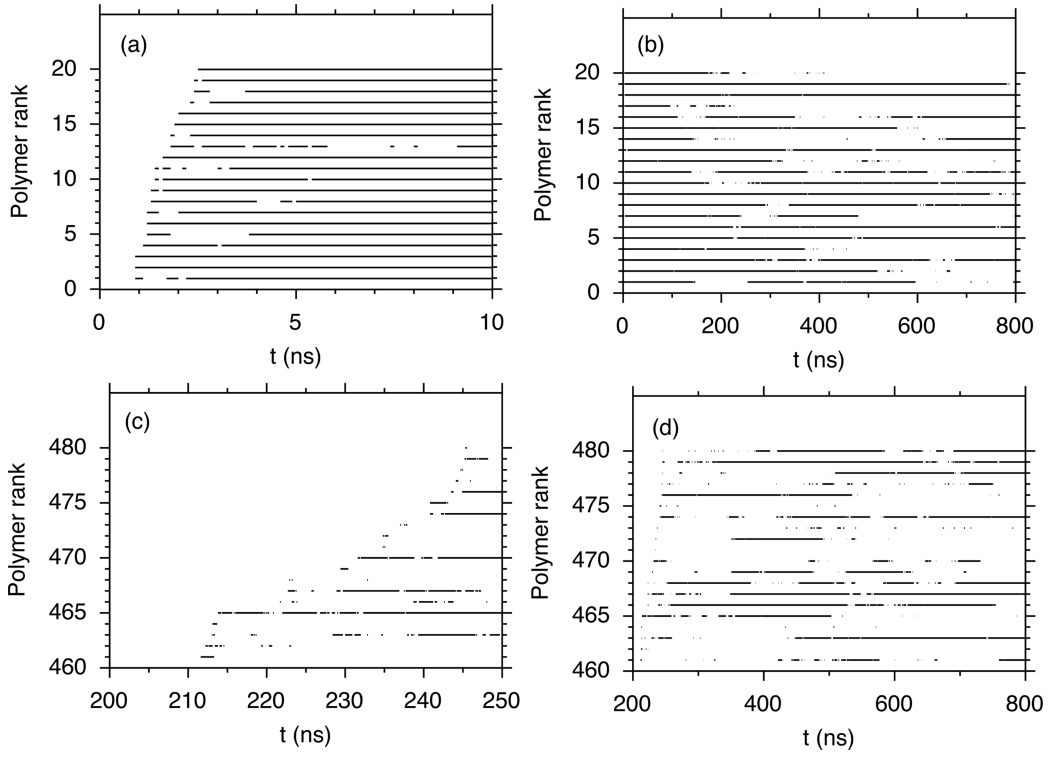

Figure 13. Adsorption history of polymers with different rank where an adsorbed state is represented by a horizontal line as as a function of simulation time of (a and b) the 20 first adsorbed polymers and (c and d) 20 polymers adsorbing after $t \approx 200$ ns for system with $k_{angle} = 0$ (flexible polymers) at $\varepsilon_s = 3.5$ kJ/mol. The abscissa scale is (a) 10 ns, (b) 800 ns, (c) 50 ns, and (d) 600 ns. Adsorption and desorption time resolution is 0.1 ns.

as compared to that of flexible polymers. Because of the extended rigid nature of the rod-like polymer, the structural rearrangement revealed by this analysis involves preferential orientation of rods with respect to the surface (rather than intrastructural rearrangements of the polymer chain as with more flexible polymers).

The time dependence of the bond ordering of the same three rod-like systems belonging to set III with the domain radius $R_\eta = 20$ Å is shown in Figure 11. First and generally, we notice that the time evolution of the bond order is only weakly dependent on the bead−surface attraction. Furthermore, we have the following time evolution: (i) The bond order is initially large, since it essentially probes beads residing in one or only a few rod-like polymers; hence, the probed beads are likely to have positively correlated bond directions. (ii) Thereafter, the bond order decreases but remains substantial, implying still a significant preferential bond orientation of the first few adsorbed polymers. (iii) At $t \approx 10$ - 20 ns, where $\tilde{N}_p^{ads}(t) \approx 0.5$, $P(\eta)$ displays a minimum. (iv) At even longer times, the bond order increases due to enhanced preferential order of nearby increasing number of adsorbed polymers. (v) At $t \approx 100$ ns the rate of the increasing bond order (still on a logarithmic time scale) is reduced. (vi) Finally, a slow relaxation occurs after $t \approx 200$ ns involving a large bond order, which enable an increased number of adsorbed polymers (cf. Figure 8f). We believe that the rate of the nematic packing (as represented by the bond order parameter) of the rod-like polymers controls the slow relaxation of $N_p^{ads}(t)$.

Thus, in addition to the slow spreading on the surface of single adsorbed polymers, an even slower adsorption mechanism appeared at adsorption from solution. For flexible polymers, this relaxation involves a lateral compression and an increased extension perpendicular to the surface originating from the osmotic pressure of the surrounding

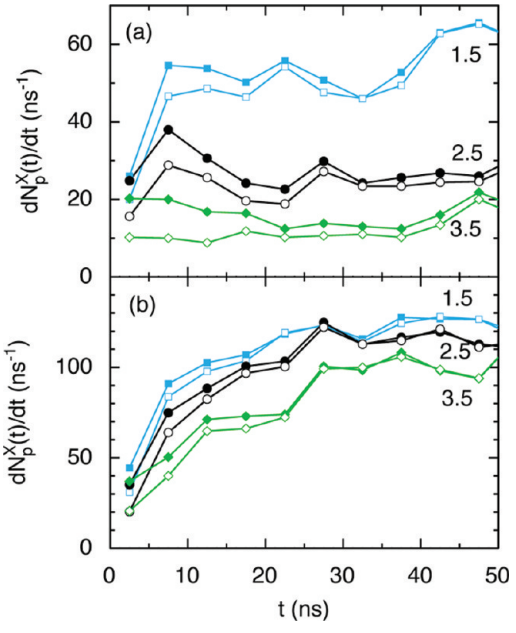

Figure 14. Number of adsorbing polymers per time unit $dN_p^{on}(t)/dt$ (solid symbols) and number of desorbing polymers per time unit $dN_p^{off}(t)/dt$ (open symbols) as a function of time t for (a) $k_{angle} = 0$ (flexible polymer, set II) and (b) $k_{angle} = 30$ J/mol deg^2 (rod-like polymer, set III) at indicated values of ε_s in kJ/mol. Adsorption and desorption time resolution is 0.1 ns, and each symbol denotes an average over 5 ns.

adsorbed polymers. Its importance becomes larger with increasing bead−surface attraction. For rod-like polymers this relaxation is slower than for flexible polymers and involve the formation of a nematic-like order of the adsorbed layer.

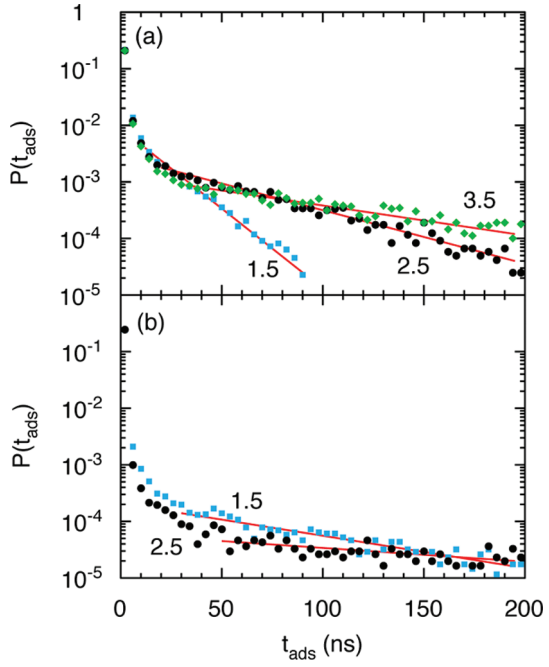

Figure 15. Probability distribution of the adsorption time $P(t_{ads})$ on a logarithmic scale for (a) $k_{angle} = 0$ (flexible polymer, set II) (b) and $k_{angle} = 30$ J/(mol deg^2) (rod-like polymer, set III) at indicated values of ε_s in kJ/mol. In part b, at $\varepsilon_s = 3.5$ kJ, the initial decay was too extended to obtain a subsequent linear regime with sufficiently accuracy. Adsorption and desorption time resolution is 0.1 ns.

4.2.3. Adsorption Dynamics of Individual Polymers. The nature of the adsorption and desorption processes of individual polymers will now be considered. Let us sort all polymers in order of increasing time of their *first* adsorption. This order number of a polymer is referred to as its rank. The adsorption history of flexible polymers with selected ranks at different time intervals of the systems with the weakest and strongest bead−surface attraction is shown in Figures 12 and 13, respectively. Panels (a) and (b) show adsorption histories of the first 20 polymers being adsorbed (i.e., at $t \approx t'$), thus describing the adsorption onto essentially a bare surface, whereas panels c and d provide adsorption histories of polymers adsorbing at the onset of an equilibrium amount of adsorbed beads (i.e., at $t \approx t''$).

As to the weak bead−surface interaction strength, polymers adsorbing at $t \approx t' \approx 1$ ns display a large variety of their fate at the surface (Figure 12a). Only a few of them are continuously adsorbed for at least 10 ns. The remaining polymers quickly desorb, whereafter most of them adsorb again, and so on, signifying a stochastic motion of one (or a few) beads around the adsorption threshold $z = z_{ads}$. Eventually, also some of these polymers become adsorbed for longer times ($t \gtrsim 5$ ns), whereas others remain unadsorbed to $t = 10$ ns. By following the same set of polymers during the full simulation (Figure 12b), we find that all the 20 selected polymers become adsorbed before $t \approx 50$ ns and remain adsorbed for at least 50 ns. Some of the polymers remain adsorbed at the end of the simulation, however all displaying periods of detachment. Thus, polymers with one (or a few) beads just passing the adsorption threshold are rarely immediately captured by its attraction to the surface. On the contrary, we have a dynamic situation where adsorbed polymers relatively easily detach from the surface, unless they have been adsorbed for a longer time.[32,20] Moving to the adsorption history starting at $t \approx t''$, we see that polymers adsorbing onto an equilibrated adsorbed layer rarely stay adsorbed (Figure 12c). Here, most of the polymers become detached after a few ns and remain unadsorbed for at least 20 to 50 ns. Following these polymers for the remaining 600 ns (Figure 12d), half of them have become adsorbed for at least 100 ns. Finally, the fact that about half of the polymers that initially adsorb at $t \approx t'$ are adsorbed at $t' = t' + 600$ ns, and a similar fraction of polymer first being adsorbed at $t \approx t''$ are adsorbed at $t' = t'' + 600$ ns suggests that polymers which become adsorbed at t' and t'' are radomized in the adsorbed layer during the rest of the simulation.

Table 4. Integration Time and Residence Time of Integrated Polymers[a]

k_{angle} (J/(mol deg^2))	ε_s (kJ/mol)	τ_{int} (ns)	τ_{res} (ns)
0	1.5	12	15
0	2.5	20	46
0	3.5	30	90
30	1.5	30	76
30	2.5	50	180

[a] The integration time τ_{int} is taken as the adsorption time at the onset where the adsorption probability distribution $P(t_{ads})$ displays an exponential behavior according to $P(t_{ads}) = Ce^{-(t_{ads}/\tau_{res})}$. The time constant τ_{res} of the exponential behavior is taken as the residence time of fully integrated polymers. Estimated uncertainties are 30% (τ_{int}) and 10% (τ_{res}).

Adsorption onto the surface with the strongest interaction strength shows that the first 20 polymers which adsorb at $t \approx t'$ are still adsorbed after 10 ns, only a few of the polymers display one or several short periods of detachment (Figure 13a). Looking further ahead, (i) all the 20 selected polymers remain adsorbed after 100 ns, (ii) most of them become detached at a later stage of the simulation, and (iii) 8−9 of them remain adsorbed essentially throughout the entire simulation (Figure 13b). Shifting focus to those polymers which become adsorbed for the first time at $t \approx t''$, only a few of these polymers become directly integrated in the adsorbed layer whereas most of them remain unadsorbed for at least 10 ns (Figure 13c); similar to that appearing at the surface with the weakest bead−surface interaction strength. On a longer time scale (Figure 14d), also here about half of the polymers become adsorbed for at least 100 ns while some have remained adsorbed throughout the simulation without any longer periods of detachment.

Thus, the nature of the adsorption with the two different bead−surface potentials displays two characteristic differences. First, at $\varepsilon_s = 1.5$ kJ/mol with $u_{surf}(z_{ads}) = -0.25k_bT$, the polymer motion at the adsorption threshold z_{ads} is strongly influenced by diffusion, whereas for $\varepsilon_s = 3.5$ kJ/mol with $u_{surf}(z_{ads}) = -0.58k_bT$ most polymers which pass the adsorption threshold are captured by a bare surface (cf. Figures 12a and 13a). Second, polymers adsorbed at the surface with the strongest bead−surface interaction strength have longer adsorption times[26] (cf. Figures 12b and 13b). Nevertheless, after $t = 800$ ns in either system there is no evidence that polymers adsorbed at $t \approx t'$ are in excess over those adsorbed at $t \approx t''$ (cf. panels b and d of Figures 12 and 13). Hence, the simulations are sufficiently long to allow early adsorbed polymers to become exchanged by other ones.

4.2.4. Adsorption Rate, Integration Time, and Residence Time. Some issues of the adsorption dynamics illustrated in Figures 12 and 13 will now be quantified on a more firm basis by statistical analysis. First, consider the adsorption rate $dN_p^{ads}(t)/dt$ and its division into two terms according to $dN_p^{ads}(t)/dt = dN_p^{on}(t)/dt - dN_p^{off}(t)/dt$, where the former term denotes the number of *adsorbing* polymers per unit time (on rate) and the latter one the number of *desorbing* polymers per unit time (off rate). Figure 14 shows the initial on and off rates for systems belonging to set II and set III. As expected,

the difference between the on and off rates is largest at short times, and the two rates become obviously statistically equal after $N_p^{ads}(t)$ has relaxed. For flexible polymers (Figure 14a), (i) the difference of the on and off rates is at most 50%, but often much smaller, (ii) the initial difference of the on and off rates increases with *increasing* bead−surface interaction strength, making up for the larger $\langle N_p^{ads} \rangle$ achieved over the similar adsorption time $t'' - t' \approx t''$, and (iii) the absolute values of the on and off rates decreases with *increasing* bead−surface interaction strength, signifying a smaller flux of adsorbing and desorbing polymers. Observation i implies that the on and off rates are significantly higher than the net adsorption rate supporting the notion that the capturing of polymers is the rate limiting step of the adsorption process (after the initial diffusion of polymers through the polymer-free region adjacent to the surface). Observation ii is consistent with a larger probability for a polymer to stay adsorbed at increasing bead−surface interaction strength as illustrated in Figures 12a and 13a.

We will now continue by considering the distribution of adsorption times of adsorbed polymers. Let the distribution function $P(t_{ads})$ denote the probability that a polymer remains (continuously) adsorbed during the time t_{ads} after it has become adsorbed. Obviously, $P(0) = 1$ and $P(\infty) = 0$. Figure 15 shows $P(t_{ads})$ on a logarithmic scale for adsorbed polymers from some of the systems belonging to set II and set III.

Generally, ln $P(t_{ads})$ vs t_{ads} shows (i) a fast initial decay down to $P(t_{ads}) \approx 10^{-3}-10^{-4}$ and (ii) thereafter a linear dependence on the adsorption time t_{ads}. The time of the onset at which $\ln P(t_{ads})$ starts to become linearly dependent on t_{ads} will be referred to as the *integration* time τ_{int}. Observation i implies that polymers with an adsorption time $t_{ads} < \tau_{int}$ have a larger probability of becoming desorbed than those polymers with an adsorption time $t_{ads} > \tau_{int}$, whereas observation ii implies that for adsorption times $t_{ads} > \tau_{int}$ the desorption process becomes a first order process and thus all adsorbed polymers with $t_{ads} > \tau_{int}$ display the *same* probability of being desorbed. Polymers with an adsorption time $t_{ads} < \tau_{int}$ are considered as not yet being fully integrated in the adsorbed layer, whereas those with $t_{ads} > \tau_{int}$ are considered as fully integrated. The slope τ_{res} of $\ln P(t_{ads})$ vs t_{ads}, $t_{ads} > \tau_{int}$, provides the *residence time* (average adsorption time) of fully integrated polymers.

Table 4 provides integration time and residence time of fully integrated polymers for the systems displayed in Figure 15. Briefly, $\tau_{int} \approx 10-50$ ns and $\tau_{res} \approx 15-200$ ns. As to the flexible polymers, τ_{int} and τ_{res} increase with increasing bead−surface adsorption strength with τ_{res} displaying a stronger dependence. Rod-like polymers have ca. 3-folded longer τ_{int} and τ_{res} as compared to flexible polymers at the same bead−surface interaction strength. Furthermore, the more pronounced initial decay of $P(t_{ads})$ (Figure 15) and the higher on and off rates but similar net rates (Figure 14b) for rod-like polymers are mutually consistent and imply that a larger fraction of newly adsorbed polymers quickly desorbs. This observation is affected by the fact that the adsorption threshold is somewhat outside the single adsorption peak for rod-like polymers (see Figure 1e).

Furthermore, the same analysis restricted to polymers adsorbing at $t < t_r$ with $t_r = 10$ ns for flexible polymers at weak bead−surface attraction and $t_r = 50$ ns for stiff polymers at strong bead−surface attraction displayed somewhat longer residence times than those given in Table 4. Hence, polymers adsorbing on a bare surface have a longer residence times than polymers adsorbing on a polymer covered surface.

An analysis of $P(t_{ads})$ for the adsorption of unconnected beads results in a purely single exponentially decaying function already from the first sampling point at $100\Delta t_{samp} = 0.1$ ns. This implies that all positions in the adsorbed region should be reached within 0.1 ns, consistent with D_0 and the thickness of the adsorbed region. Hence, this unconnected bead analysis is consistent with the notion of an integration time for polymer adsorption, and we conceive that the integration involves a penetration of a newly adsorbed polymer to the surface to become fully anchored.

Hence, we have defined the time for a polymer to become fully integrated into the adsorbed layer. Moreover, it was found that the integration time and the residence time of fully integrated polymers increase with increasing polymer stiffness and increasing bead−surface interaction strength.

5. Discussion

5.1. Equilibrium Properties. We start our discussion of the equilibrium properties with the two observations that if everything else is equal, the *bead* adsorption is promoted by (A) increasing bead−surface attraction and (B) increasing polymer stiffness (Figure 2a). Generally, polymers that adsorb to solid surfaces loose conformational degrees of freedom due to a more restricted set of conformations allowed in the adsorbed state. Hence, polymer adsorption requires that the adsorption energy exceeds this entropy penalty associated with the loss of conformations and thus a stronger adsorption energy promotes a higher degree of adsorption, explaining observation A. Furthermore, an increasing stiffness of a polymer reduces its conformational degrees of freedom. Since, this loss is larger in solution than in the adsorbed state, a stiffer polymer looses less conformational entropy than a flexible one upon adsorption. Thus, given that the adsorption energy exceeds the entropy loss upon adsorption, stiffer polymers adsorb stronger than flexible ones, which explains observation B.

Interestingly, and not covered by arguments A and B, the number of adsorbed beads decreases slightly upon increasing stiffness for persistence length up to $l_p \approx 15$ Å, Presently, we have no unambiguous explanation for this. A similar but more distinct minimum was earlier found by van Eijk and Leermakers for the adsorption of polymers at liquid−liquid interfaces of variable width using a lattice mean-field theory.[41]

We now continue with the finding that (C) the number of adsorbed polymers displays a maximum upon increasing polymer stiffness at the persistence length $l_p = 20-30$ Å (Figure 2b). Mechanistically, observation C could be explained as follows. At increasing stiffness of an adsorbed polymer, the fraction of adsorbed beads is approximately constant or increased (Figure 4c). This increase dominates over the increase in the number of adsorbed beads (Figure 2a) for sufficiently stiff polymers, which makes the number of adsorbed polymers to decrease with increasing stiffness. Flexible to semiflexible polymers up to a persistence length of $l_p = 20-30$ Å, however, constitute an exception. For these polymers, the fraction of adsorbed beads is not increasing rapidly enough to dominate over the increasing number of adsorbed beads at increasing stiffness. These two aspects together establish a background for observation C.

On a more profound level, we propose that observation C is related to the similar maxima of the perpendicular extension (Figure 3a) and of the number of beads in tails (Figure 4a). Moreover, they could collectively be understood as originating from two competing effects. (i) At increasing stiffness, an adsorbed polymer coil becomes expanded as

compared to a flexible one, and the larger surface pressure associated with this forces the coil to extend perpendicular to the surface. (ii) Stiff chains prefer to adsorb parallel to the surface making the perpendicular extension small. Hence, when effect of the expansion is balanced by the tendency of a parallel adsorption, we expect maxima in the number of adsorbed polymers, perpendicular extension, and number of beads in tails.

The width of the adsorbed layer is only 2−3 Å for rod-like polymers, but 6−7 Å for flexible ones (Figure 1a). This supports the conception that flexible polymers retain much of their conformational degrees of freedom in the adsorbed state. The bond order analysis (Figure 5) and snapshots (Figure 6) clearly demonstrate the disordered adsorbed state of the flexible polymers along with the nematic order of the rod-like polymers. We have not made a systematic extension of our simulations to see if the defects of the nematic order observed are a result of insufficient length of the simulations or true equilibrium properties of the systems.

5.2. Dynamic Properties. The sequence of the adsorption phases appearing for the adsorption of a *single* polymer under different polymer flexibilities and adsorption strengths has previously been described[31] using a similar approach. There we divided the adsorption into three consecutive phases with increasing time scales: (i) initial distortion phase, where the polymer becomes deformed by its weak attraction to the solid surface, (ii) attachment phase where the polymer starts to physically attach to the surface and partly spread on it, and (iii) relaxation phase where the adsorbed polymer attains full in-plane equilibrium. For a flexible 20-bead long polymer at the intermediate bead−surface interaction strength, the lengths of the three phases were 2, 20, and 50 ns, respectively.

Here, we have in more detail examined the appearance of additional structural relaxation mechanisms appearing during the adsorption of polymers from good solvent. We have found that for flexible polymers a reduction of the parallel extension appears at a late stage of the adsorption. Maximal parallel component of the radius gyration, minimum number of beads in tails (Figure 9a), and maximum number of beads in trains (Figure 9c) appear about $t = 20-30$ ns, thus *interfering* the final parallel relaxation appearing for isolated adsorbed polymers. This fourth relaxation mechanism lasts for $t \approx 100-200$ ns. The relaxation time increases with increasing bead−surface interaction strength. The similarity of the relaxation time of this fourth phase and t'' of the number of adsorbed polymers makes it tentative to conclude that the increased surface pressure of the increasing number of polymers drives this conformational change of adsorbed polymers. Such a final relaxation mechanism of flexible polymers adsorbing onto solid surfaces involving an increased thickness of the adsorbed polymer layer has previously been deduced from experimental adsorption studies by Fu and Santore,[39] predicted by Hasegawa and Doi using mean-field theory,[18] and seen in our previous study with $\varepsilon_s =$ 2.5 kJ/mol.[32] Here, we have have shown that this final structural relaxation becomes more important at increasing bead−surface attraction and prominent at strong bead−surface attraction.

The final structural relaxation mechanism of the adsorption of rod-like polymers is of a different nature. We have seen that the relaxation of the radius of gyration and of tail, loop, and train characteristics now become monotonic with longer time relaxation times as compared to flexible polymers. Moreover, the relaxation of adsorbed polymers displays a long tail after an initial adsorption of similar rate as for flexible polymers. Our analysis points to that the final relaxation toward full equilibrium involves the formation of larger domains of nematic order in the adsorbed polymer layer. The formation of such domains develops on a time scale comparable to the full simulation length (Figure 11). This process appears to be completed for the weakest bead−surface interaction; however, a slight disagreement among the MC data with $R_\eta > 20$ Å for $\varepsilon_s = 2.5$ and 3.5 kJ/mol (data not shown) indicates that we have not yet reached complete equilibrium structures at these conditions and confirms the slow merging of domains with different nematic directions both in the MC and BD simulations.

By examination of the probability function of adsorption times, we have (i) found that newly adsorbed polymers are more likely to desorb than polymers that have been adsorbed for a longer time, (ii) defined and determined integration times for polymers to become fully integrated in the adsorbed layer, and (iii) determined the residence time of fully integrated polymers.

The observed increase of integration time and residence time of fully integrated polymers at increasing effective polymer−surface attraction (achieved by either increasing bead−surface attraction at fixed polymer stiffness or increased polymer stiffness at fixed bead−surface attraction) could be understood as follows. At increasing effective polymer−surface attraction, the number of adsorbed bead increases (Figure 2a). This will reduce the space available and concomitantly reduce the probability for a newly and energetically weakly adsorbed polymer to become more firmly anchored, and hence τ_{int} increases. Furthermore, polymers already integrated in the adsorbed layer become more strongly adsorbed making them less likely to desorb and hence τ_{res} increases.[40]

Finally, the integration and residence times are well determined as long as the sampling interval of adsorbed polymers is not too coarse. However, the magnitude of the initial drop in the probability distribution of the adsorption time is affected by the sampling interval.

6. Conclusions

Adsorption of uncharged 20-mers onto planar surfaces from a good solvent has been studied for various bead−surface attractions and different intrinsic stiffnesses of the polymers. Equilibrium adsorption properties of 40 systems were determined by Monte Carlo simulations, and the adsorption processes of 16 of these were determined by Brownian dynamic simulations.

Static and dynamic properties of the polymers were analyzed by monitoring bead and polymer density profiles, parallel and perpendicular components of the radius of gyration, number of beads residing in tails, loops, and trains, and degree of nematic bond order of the adsorbed layer. Furthermore, adsorption and desorption rates as well as integration time and residence time of fully integrated polymers have been determined. The integration time is taken as the adsorption time needed to obtain a first order desorption kinetics. Our main conclusions are as follows:

(A) For the flexible polymers, the adsorbed structure involved two polymer layers, whereas for stiff polymers only a single polymer layer was formed.

(B) At increasing stiffness, the number of adsorbed polymers, the extension of the adsorbed polymers perpendicular to the surface and the number of beads in tails displayed a maximum. These extreme points are proposed to be related and a balance of the general expansion of polymer coils at increasing

stiffness and the propensity for parallel adsorption of stiff polymers.

(C) In addition to the slow spreading on the surface of single adsorbed polymers, an even slower adsorption mechanism appeared at adsorption from solution of flexible polymers. This relaxation involves a lateral compression and an increased extension perpendicular to the surface originating from the osmotic pressure of the surrounding adsorbed polymers. Its importance becomes larger with increasing bead−surface attraction.

(D) The final relaxation mechanism appearing at adsorption from solution of rod-like polymers was even slower than for flexible polymers and involved the formation of a nematic-like order of the adsorbed layer.

(E) Disregarding the initial adsorption, the net adsorption rate was controlled by the low probability of newly adsorbed polymers to become integrated in the adsorbed layer.

(G) The time for a polymer to become fully integrated into the adsorbed layer was defined. This integration time and the residence time of fully integrated polymers increase with increasing polymer stiffness and increasing the bead−surface interaction strength.

Acknowledgment. The authors thank Center for Scientific and Technical Computing at Lund University (LUNARC) for generous allocation of computer resources. Financial support by the Swedish Research Council (VR) is also gratefully acknow ledged.

References and Notes

(1) Fleer, G. J.; Lyklema, J. *Adsorption From Solution at the Solid/Liquid Interface*; Academic Press: New York, 1983.
(2) Evans, D. F.; Wennerström, H. *The Colloidal Domain: Where Physics, Chemistry, Biology and Technology Meet*, 2nd ed.; Wiley-VCH: New York, 1999.
(3) Norde, W. *Colloids and Interfaces in Life Sciences*; Marcel Dekker Inc.: New York, 2003.
(4) Gray, J. J. *Curr. Opin. Struc. Biol.* **2004**, *14*, 110.
(5) Yaseen, M.; Salacinski, H. J.; Seifalian, A. M.; Lu, J. R. *Biomed. Mater.* **2008**, *3*, 034123.
(6) Ramanathan, T.; Abdala, A. A.; Stankovich, S.; Dikin, D. A.; Herrera-Alonso, M.; Piner, R. D.; Adamson, D. H.; Schniepp, H. C.; Chen, X.; Ruoff, R. S.; et al. *Nat. Nanotechnol.* **2008**, *3*, 327.
(7) Fleer, G. J.; Cohen Stuart, M. A.; Scheutjens, J. H. M. H.; Cosgrove, T.; Vincent, B. *Polymers at Interfaces*; Chapman & Hall: London, 1993.
(8) Cohen Stuart, M. A.; Fleer, G. J. *Annu. Rev. Mater. Sci.* **1996**, *26*, 463.
(9) Yethiraj, A. *Adv. Chem. Phys.* **2002**, *121*, 89.
(10) Cohen Stuart, M. A. *Surf. Sci. Ser.* **2003**, *110*, 1.
(11) O'Shaughnessy, B.; Vavylonis, D. *J. Phys.: Condens. Matter* **2005**, *17*, R63.
(12) Scheutjens, J. M. H. M.; Fleer, G. J. *J. Phys. Chem.* **1980**, *84*, 178.
(13) de Gennes, P. G. *Macromolecules* **1981**, *14*, 1637.
(14) Kramarenko, E. Yu.; Winkler, R. G.; Khalatur, P. G.; Khokhlov, A. R.; Reineker, P. *J. Chem. Phys.* **1996**, *104*, 4806.
(15) Striolo, A.; Prausnitz, J. M. *J. Chem. Phys.* **2001**, *114*, 8565.
(16) Sintes, T.; Sumithra, K.; Straube, E. *Macromolecules* **2001**, *34*, 1352.
(17) Striolo, A.; Jayaraman, A.; Genzer, J.; Hall, C. K. *J. Chem. Phys.* **2005**, *123*, 064710.
(18) Hasegawa, R.; Doi, M. *Macromolecules* **1997**, *30*, 3086.
(19) Jia, L.-C, R.; Lai., P. Y. *J. Chem. Phys.* **1996**, *105*, 11319.
(20) Zajac, R.; Chakrabarti, A. *J. Chem. Phys.* **1996**, *104*, 2418.
(21) Takeuchi, H. *Macromol. Theory Simul.* **1999**, *8*, 391.
(22) Ponomarev, A. L.; Sewell, T. D.; Durning, C. J. *Macromolecules* **2000**, *33*, 2662.
(23) Wolterink, J. K.; Barkema, G. T.; Cohen Stuart, M. A. *Macromolecules* **2005**, *38*, 2009.
(24) Smith, G. D.; Zhang, Y.; Yin, F.; Bedrov, D. *Langmuir* **2006**, *22*, 664.
(25) Descas, R.; Sommer, J.-U.; Blumen, A. *J. Chem. Phys.* **2006**, *124*, 094701.
(26) Smith, K. A.; Vladkov, M.; Barrat, J.-L. *Macromolecules* **2005**, *38*, 571.
(27) Harmandaris, V. A.; Daoulas, K. Ch.; Mavrantzas, V. G. *Macromolecules* **2005**, *38*, 5796.
(28) Daoulas, K. Ch; Harmandaris, V. A.; Mavrantzas, V. G. *Macromolecules* **2005**, *38*, 5780.
(29) Li, Y.; Wei, D.; Han, C. C.; Liao, Q. *J. Chem. Phys.* **2007**, *126*, 204907.
(30) Chremos, A.; Glynos, E.; Koutsos, V.; Camp, P. J. *Soft Matter* **2009**, *5*, 637.
(31) Källrot, N.; Linse, P. *Macromolecules* **2007**, *40*, 4669.
(32) Källrot, N.; Dahlqvist, M.; Linse, P. *Macromolecules* **2009**, *42*, 3641.
(33) Baschnagel, J.; Mayer, H.; Varnik, F.; Metzger, S.; Aichele, M.; Müller, M.; Binder, K. *Interface Sci.* **2003**, *11*, 159.
(34) Ullner, M.; Jönsson, B.; Peterson, C.; Sommelius, O.; Söderberg, B. *J. Chem. Phys.* **1997**, *107*, 1279.
(35) Akinchina, A.; Linse, P. *Macromolecules* **2002**, *35*, 5183.
(36) MOLSIM, Version 4.7, Linse, P.; Lund University: Sweden, 2009.
(37) Allen, M. P.; Tildesley, D. J. *Computer Simulations of Liquids*; Oxford University Press: Oxford, England, 1987.
(38) Ermak, D. L.; McCammon, J. A. *J. Chem. Phys.* **1978**, *69*, 1352.
(39) Fu, Z.; Santore, M. *Macromolecules* **1999**, *32*, 1939.
(40) Sukhishvili, S. A.; Chen, Y.; Müller, J. D.; Gratton, E.; Schweizer, K. S.; Granick, S. *Macromolecules* **2002**, *35*, 1776.
(41) van Eijk., M. C. P.; Leermakers, F. A. M. *J. Chem. Phys.* **1998**, *109*, 4592.